Geometrical renormalization approach to calculating optical properties of fractal carbonaceous soot

VADIM A. MARKEL[1] AND VLADIMIR M. SHALAEV[2]

[1]Department of Electrical Engineering, Washington University, St. Louis, MO 63130
[2]Department of Physics, New Mexico State University, Las Cruces, NM 88003

Compiled August 15, 2023

We develop a theoretical approach to calculating optical properties of carbonaceous soot in the long-wavelength limit. Our method is based on geometrical renormalization of clusters; it avoids both the inaccuracy of the dipole approximation in its pure form and the numerical complexity of rigorous direct methods of solving the EM boundary problem. The results are verified by comparison with experimental measurements for specific extinction of diesel soot in the spectral region from 0.488μm to 0.857cm performed by Bruce *et al.* [*Appl.Opt.*, 30, 1537 (1991)]. The theory leads to analytical expressions that are applicable to different soots, with various geometrical properties and optical constants. We show that the functional form of the long-wavelength asymptote of the specific extinction can critically depend on a parameter characterizing the sample geometry and identify the critical value of this parameter.

OCIS codes: (010.1110) Aerosols; (290.1090) Aerosol and cloud effects; (290.2200) Extinction; (290.3770) Long-wave scattering

J. Opt. Soc. Am. A **18**, 1112-1121 (2001); https://doi.org/10.1364/JOSAA.18.001112

1. INTRODUCTION

A. Review of the problem

Understanding the optical properties of carbonaceous soot in a wide spectral range is important for many application areas, such as climate research, monitoring of atmospheric pollution, remote sensing of fires, to name just a few. It has been long recognized [1–4] that aerosol soot consists of fractal clusters built of many hundreds or thousands of little nanometer-scale carbon spheres (monomers), and the geometrical structure of soot plays an important role for optical properties. In the visible and near-infrared spectral regions the electromagnetic interaction of monomers in a soot cluster is relatively weak, and analytical perturbative approaches such as the mean-filed approximation [5] produce sufficiently accurate results. However, as the wavelength is further increased, the optical constants of black carbon become more "metallic-like" (dominated by the input of conduction electrons) [6] which leads to stronger electromagnetic interaction and the eventual breakdown of the perturbative methods. As a result, the collective optical properties of a soot cluster become increasingly different from those of isolated monomers [7, 8]. Experimental measurements of absorption and extinction efficiencies of diesel soot in a very wide spectral range (from 0.5μm to 0.857cm) [9] demonstrated that neither the model of isolated spheres nor of long cylinders can explain the spectral dependence of the above quantities.

The nonperturbative methods that can account for strong electromagnetic interaction in the long-wavelength spectral region include the dipole approximation [5, 10–13] and the family of rigorous numerical methods in which the field scattered by each monomer is expanded into spherical harmonics up to a certain maximum order [8, 14–19]. However, both methods have shortcomings. The dipole approximation for aggregated spheres is accurate only when the spheres are separated by distances larger than their diameters, or the electromagnetic interaction is weak (the latter situation took place, for example, in Ref. [5]). The general non-applicability of the dipole approximation to arrays of strongly interacting touching spheres was verified both theoretically [14, 15] and experimentally [20]. A simple physical explanation of why the dipole approximation fails was provided, for example, in Ref. [20].

A rigorous numerical approach to solution of the Maxwell equations for touching spheres has been developed by different authors [8, 14–19]. The essence of this method, which can be referred to as the "coupled multipoles" method, is to expand the EM field inside each sphere and the field scattered by each sphere in vector spherical harmonics, and to match the boundary condition on all surfaces of discontinuity. Generally, this method leads to an infinite-dimensional system of linear equations with respect to the expansion coefficients. In order to solve this system, one needs to truncate it by assuming that all the expansion coefficients for spherical harmonics of the order larger than L are zero. Then the total number of equations scales (for large values of L) as NL^2. Although this method

gives a rigorous numerical solution to the Maxwell equations in the limit $L \to \infty$, it has a fundamental difficulty: when the interaction of monomers in a cluster becomes stronger and the perturbation expansion, correspondingly, less accurate (or even diverges), the number L required for attaining accurate results tends to increase [21, 22]. This feature is illustrated in Fig. 3 below. On the other hand, the number N should stay sufficiently large in order to retain the fractal geometry of samples.

To overcome the inadequacy of the dipole approximation and the overwhelming computational complexity of the coupled multipole method, we have suggested the geometrical cluster renormalization method (GCRM) [23, 24]. This approach allows one to stay in the frame of the dipole approximation. This paper is focused on application of this method to carbonaceous soot in the spectral range from, approximately, 0.5μm to 1cm. The results are compared with experimental measurements reported by Bruce *et al.* [9].

The major advantage of the GCRM is numerical simplicity. But, in addition to that, useful analytical results can be obtained in an approximation where the retardation effects are ignored (the quasistatic limit) and the weighted density of states (WDS) of the dipole interaction operator is replaced by a step function. These two approximations lead to an analytical formula which is very accurate (as verified by comparison to results of direct numerical calculations within the GCRM) for materials such as black carbon in the spectral range from the near IR to centimeter waves. The availability of an analytical expression allows one to investigate the dependence of the spectra on important parameters of the problem and to make conclusions of a more general applicability.

B. Optical constants of black carbon

Any numerical or analytical calculation requires the knowledge of optical constants of the soot material. Unfortunately, there is some uncertainty in this matter. Black carbon can exist in several modifications (graphite, amorphous, glassy carbon). We will use the data by Dalzell and Sarofim [6] who proposed a three-electron dispersion formula for optical constants and verified it experimentally in the spectral range $0.4\mu\text{m} < \lambda < 10\mu\text{m}$. The availability of an analytic expression for the optical constants allowed us to extrapolate them into a much wider spectral range. The important feature of this dispersion formula is the presence of a free-electron term which dominates the optical constants at large wavelengths.

The dispersion formula for the dielectric constant ϵ suggested by Dalzell and Sarofim is based on the well-known quantum expression for the complex dielectric function:

$$\epsilon(\omega) = 1 - \sum_n \frac{f_n^2}{\omega^2 - \omega_n^2 + i\gamma_n\omega} \,. \qquad \textbf{(1)}$$

Earlier, Taft and Philipp [25] identified experimentally three optical resonances in graphite, two of which correspond to bound electrons and one to conduction electrons. The resonance frequencies are $\omega_c = 0$ (conduction electrons), $\omega_1 = 1.25 \cdot 10^{15}\text{sec}^{-1}$ and $\omega_2 = 7.25 \cdot 10^{15}\text{s}^{-1}$ (or corresponding wavelengths: $\lambda_c = \infty$, $\lambda_1 = 1.51\mu$m, $\lambda_2 = 0.26\mu$m). The values of the relaxation constants were found to be $\gamma_c = \gamma_1 = 6.00 \cdot 10^{15}\text{s}^{-1}$, $\gamma_2 = 7.25 \cdot 10^{15}\text{s}^{-1}$. Dalzell and Sarofim assumed that the same electronic transitions contribute to the dielectric constant of carbon soot and used the above values of ω_n and γ_n to fit the formula (1) to their experimental data treating f_n's (which depend on concentration of optically active electrons) as free

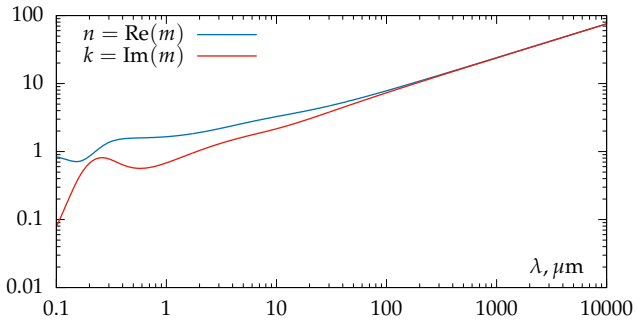

Fig. 1. Real and imaginary parts of the complex refraction index $m = \sqrt{\epsilon} = n + ik$ as functions of wavelength calculated using dispersion formula (1).

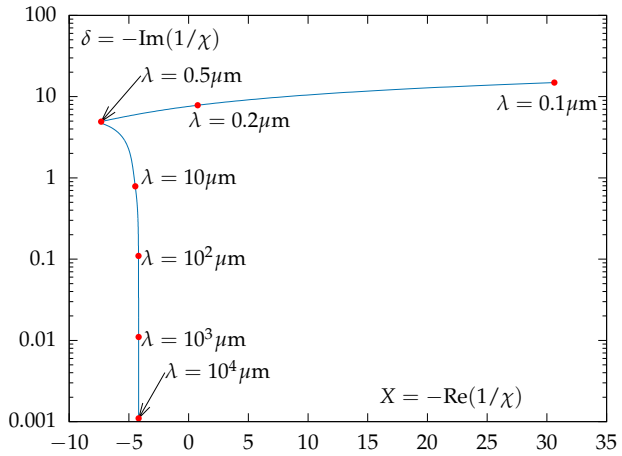

Fig. 2. Spectral dependence of the complex variable $1/\chi = -(X + i\delta)$ parameterized by the wavelength λ, where $\chi = (3/4\pi)(\epsilon - 1)/(\epsilon + 2)$.

parameters. A very accurate fit to the experimental data for propane soot was achieved for the following values of f_n: $f_c = 4.04 \cdot 10^{15}\text{s}^{-1}$, $f_1 = 2.93 \cdot 10^{15}\text{sec}^{-1}$, $f_2 = 9.54 \cdot 10^{15}\text{s}^{-1}$ in the spectral range $0.4\mu\text{m} < \lambda < 10\mu\text{m}$. Analogous three-electron dispersion formulas were used to describe optical constants of smoke at the flame temperatures [26]. The temperature dependence is mainly governed by the temperature dependence of the conduction electron relaxation constant: [27] $\gamma_c \propto T^{1/2}$.

The real and imaginary parts of the complex refraction index $m = \sqrt{\epsilon} = n + ik$ calculated from formula (1) with the constants specified above are shown in Fig. 1. The low-frequency metallic behavior of the optical constants is clearly manifested for $\lambda > 100\mu$m: n and k become very close to each other and scale with wavelength as $\sqrt{\lambda}$. Mathematically, this happens when the term $if_c^2/\gamma_c\omega$ becomes dominant in (1), i.e., for $\omega \ll \gamma_c$.

In Fig. 2 we also show the spectral dependence of two important optical parameters, X and δ, originally introduced [28] in Refs. [10, 11]. They are defined as $X = -\text{Re}[1/\chi]$, $\delta = -\text{Im}[1/\chi]$, where

$$\chi = \frac{3}{4\pi}\frac{\epsilon - 1}{\epsilon + 2} \,. \qquad \textbf{(2)}$$

The physical meaning of these parameters is that X is the generalized detuning from the resonance and δ - the generalized dielectric loss parameter.

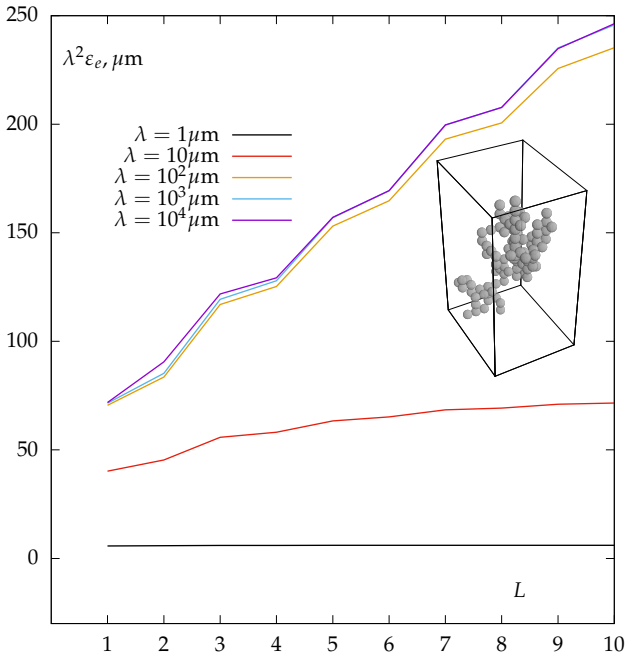

Fig. 3. Specific extinction ε_e, multiplied by λ^2 and averaged over spatial rotations, as a function of L (Fortran codes courtesy of D. Mackowski). The calculations were performed in the quasistatic limit for a 3D cluster-cluster aggregate of $N = 100$ touching spheres shown in the inset.

C. Convergence of the coupled multipoles method

The breakdown of the dipole approximation for clusters of touching spheres happens even when the overall size of the clusters is much smaller that the wavelength and the usual quasistatic methods apply [8, 29]. In principle, this problem can be resolved by using rigorous numerical solution to the Maxwell equations [8, 14, 29]. However, the convergence of these methods with the maximum order of spherical harmonics used (L) is a major problem for large clusters. The number of linear equations that must be solved in this approach scales as NL^2 where N is the number of primary spheres. In this subsection we demonstrate that such convergence cannot be realistically achieved for $\lambda > 10\mu$m.

We have used in our calculations a model fractal cluster of $N = 100$ primary spheres. The cluster was generated using the cluster-cluster aggregation process [30, 31] in 3D. We have calculated the specific extinction ε_e (per unit volume) defined as

$$\varepsilon_e = \sigma_e / V_{\rm tot} \,, \tag{3}$$

where σ_e is the total extinction cross section and $V_{\rm tot}$ is the total volume of the cluster (equal to N times the volume of primary spheres, v). Quasistatic Fortran codes courtesy of D.W. Mackowski were used in the calculations (see Refs. [8, 29] for more details), and the refractive index was calculated using (1).

The results are presented in Fig. 3 where we plot the quantity $\lambda^2\varepsilon_e$ as a function of L for different wavelengths. The specific extinction is multiplied by λ^2 so that the data for different λ's can all be compared in the same plot. It can be seen that a fast convergence is reached for $\lambda = 1\mu$m. (The scale of this figure does not allow one to see that the convergence is, in fact, achieved for $L > 4$ at this wavelength). The convergence for $\lambda = 10\mu$m is somewhat slower. It is, actually, difficult to judge from the figure if the result can still change considerably with increasing L.

But for the wavelengths $\lambda = 10^2, 10^3$ and $10^4\mu$m, when the refractive index of carbon is metallic (see Fig. 1), the convergence is not achieved at all. The quantity $\lambda^2\varepsilon_e$ grows linearly with L and does not depend noticeably on λ. Extrapolating the linear growth of $\lambda^2\varepsilon_e$ to larger values of L, and using experimental values of the the specific extinction, we can roughly estimate the lower bound of L that is required for convergence. From experimental data of Bruce *et al* [9] we find that $\varepsilon_e \approx 0.13\mu\text{m}^{-1}$ for $\lambda \approx 100\mu$m (to obtain this result, we have used the mass density of black carbon $\rho \approx 2\text{g/cm}^3$; specific extinction in Ref. [9] is measured per unit of mass rather than volume). Thus, at $\lambda \approx 100\mu$m, we have $\lambda^2\varepsilon_e \approx 1300\mu$m. The linear growth of $\lambda^2\varepsilon_e$ as a function of L in Fig. 3 can be approximated by $\lambda^2\varepsilon_e = [50 + 20L]\mu$m. If this linear behavior is extrapolated to larger values of L, the experimental value of $\lambda^2\varepsilon_e$ is reached at $L \approx 65$. However, it is plausible to assume that the slope of the curve $\lambda^2\varepsilon_e(L)$ will decrease for larger L, and the actual number of spherical harmonics necessary for convergence is larger than 65. Even for $L \approx 65$ and $N = 100$, the number of equations that must be solved is 422,500. And a larger L is required for $\lambda > 100\mu$m. This makes the direct numerical approach impractical for large wavelengths.

It can be seen in Fig. 3 that the dependence $\varepsilon_e(L)$ has a form of a ladder with alternating steps of different heights. For example, $\varepsilon_e(4) - \varepsilon_e(3)$ is much smaller than $\varepsilon_e(5) - \varepsilon_e(4)$. Therefore, it is generally incorrect to stop iterations at a certain value of L when the change in ε_e is less than some small constant. Instead, this condition should hold for two consecutive iterations. Also, even if the above condition is met, it is not always clear that a relatively large change in ε_e will not accumulate for larger values of L. Thus, the convergence criterion should be not the small change in ε_e after two consecutive iterations, but rather a manifested plato in the curve $\varepsilon_e(L)$.

2. THEORY

A. Dipole approximation

In this subsection we briefly describe the dipole approximation in its generic form and introduce the relevant notations.

The essence of the dipole approximation is to replace each (finite size) monomer in a cluster by a point dipole with polarizability α, located at the point $\mathbf{r}_i$ at the center of the respective spherical monomer. The dipole moment of the ith monomer, $\mathbf{d}_i$, is proportional to the local field at the point $\mathbf{r}_i$ which is a superposition of the incident field and all the secondary fields scattered by other dipoles. Therefore, the dipole moments of the monomers are coupled to the incident field and to each other as described by the coupled dipole equation (CDE):

$$\mathbf{d}_i = \alpha \left[\mathbf{E}_{\rm inc}(\mathbf{r}_i) + \sum_{j \neq i}^{N} \hat{G}(\mathbf{r}_i - \mathbf{r}_j)\mathbf{d}_j \right] . \tag{4}$$

Here the term $\hat{G}(\mathbf{r}_i - \mathbf{r}_j)\mathbf{d}_j$ gives the dipole radiation field created by the dipole $\mathbf{d}_j$ at the point $\mathbf{r}_i$ and $\hat{G}(\mathbf{r})$ is the regular part of the free space dyadic Green's function:

$$G_{\alpha\beta}(\mathbf{r}) = k^3 \left[A(kr)\delta_{\alpha\beta} + B(kr) r_\alpha r_\beta / r^2 \right] , \tag{5}$$

$$A(x) = [x^{-1} + ix^{-2} - x^{-3}] \exp(ix) \,, \tag{6}$$

$$B(x) = [-x^{-1} - 3ix^{-2} + 3x^{-3}] \exp(ix) \,, \tag{7}$$

where $k = 2\pi/\lambda$ is the wavenumber, $(\hat{G}\mathbf{d})_\alpha = G_{\alpha\beta}d_\beta$, the Greek indices stand for the Cartesian components of vectors and summation over repeated indices is implied.

The CDE is a system of $3N$ linear equations that can be solved to find the dipole moments $\mathbf{d}_i$. The cross sections of extinction and absorption can be found from the optical theorem:

$$\sigma_e = \frac{4\pi k}{|\mathbf{E}_0|^2}\mathrm{Im}\sum_{i=1}^{N}\mathbf{d}_i\cdot\mathbf{E}^*_{\mathrm{inc}}(\mathbf{r}_i)\,, \tag{8}$$

$$\sigma_a = \frac{4\pi k}{|\mathbf{E}_0|^2}y_a\sum_{i=1}^{N}|\mathbf{d}_i|^2\,, \tag{9}$$

$$y_a = -\mathrm{Im}\left(\frac{1}{\alpha}\right) - \frac{2k^3}{3} \geq 0\,. \tag{10}$$

For monomers small compared to λ, the polarizability α is given by [32]:

$$\frac{1}{\alpha} = \frac{1}{v\chi} - i\frac{2k^3}{3}\,, \tag{11}$$

where $v = (4\pi/3)R_m^3$ is the volume of a spherical monomer, R_m its radius and the susceptibility χ is defined by (2). As follows from (10), (11) and (2), y_a is non-negatively defined for any physically reasonable ϵ. The ratio $3y_a/2k^3$ characterizes the relative strength of absorption by a single isolated monomer.

B. The geometrical renormalization of clusters

In this subsection we describe the geometrical cluster renormalization method (GCRM) and its application in the dipole approximation.

First, we note that most calculations employ computer-generated samples. The geometry of these samples does not coincide with that of experimental soot exactly (which is, obviously, impossible), but rather reproduces certain statistical geometrical properties of the real soot. Among such properties are density correlation functions, total volume of the material, $V_{\mathrm{tot}} = Nv$, and average radius of gyration, R_g. However, such characteristics as the number of monomers in a cluster, N, and monomer radius, R_m, might be considered as *not essential*. It is known, for example, that the real carbon monomers are not actually spherical, and nearest neighbors touch each other not just at one geometrical point, so that the model of touching spheres is only an idealization.

Second, as was mentioned above, the dipole approximation in its pure form underestimates the strength of electromagnetic interactions between the monomers. In particular, it predicts the shift of the resonance frequency in small clusters of spheres to be significantly less than the experimentally measured [20]. In order to correct the interaction strength of the dipole approximation, we can move the monomers closer to each other (of course, this refers to computer-generated samples) by allowing them to intersect geometrically. However, doing this will evidently reduce the overall system size (R_g) which is an essential parameter of the problem. The other possible way to introduce the intersections is to increase the radiuses of the spheres (R_m) while keeping distance between nearest neighbors (l) unchanged. This will however, lead to an increase of the total volume of the material. Luckily, for fractal clusters, it is possible to introduce a simultaneous renormalization of the sphere radiuses (R_m), the total number of monomers (N) and the distance between the nearest neighbors (l) in such a way that the overall volume (V_{tot}) and the gyration radius (R_g) are unchanged, and to introduce an arbitrary geometrical intersection of neighboring spheres. The transformation is

$$R'_m = R_m\left(\frac{\xi}{2}\right)^{D/(3-D)}\,, \tag{12}$$

$$N' = N\left(\frac{2}{\xi}\right)^{3D/(3-D)}\,, \tag{13}$$

$$l' = \xi R'_m\,, \tag{14}$$

where ξ is an intersection parameter ($1 < \xi < 2$, $\xi = 2$ for touching spheres and $\xi < 2$ for geometrically intersecting spheres). Indeed, it is easy to verify that the gyration radius, which scales with l and N as

$$R_g \propto lN^{1/D}\,, \tag{15}$$

and the total volume, which scales with R_m and N as

$$V_{\mathrm{tot}} \propto NR_m^3\,, \tag{16}$$

do not change under the set of transformations defined by (12-14).

Thus, the main idea of the renormalization approach is to model an ensemble of real cluster with experimental values of R_m and N and $l = 2R_m$ by a computer-generated "renormalized" ensemble with corresponding parameters R'_m, N' and with the geometrical intersection of neighboring spheres: $l' = \xi R'_m < 2R'_m$. It is important to emphasize that the renormalization does not apply to a single random cluster, because it changes not only the inter-particle separation but also the number of particles in an individual cluster, but is rather an operation that creates the renormalized random ensemble for a given original (experimental) ensemble.

The initial value for ξ can be obtained by analogy with the discrete dipole approximation (see Refs. [32–34]) in which bulk non-spherical particles are modeled by arrays of point dipoles located on a cubic lattice. In the first approximation, the polarizability of the dipoles is taken to be equal to that of an equivalent sphere with the radius R_m such that its volume is equal to the volume of a lattice cell, i.e., $(4\pi/3)R_m^3 = l^3$. From this equality we find $\xi = l/R_m = (4\pi/3)^{1/3} \approx 1.612$.

Another approach to estimating the parameter ξ is based on the following consideration, which can be also used to justify the physical plausibility of the renormalization method. It can be shown [35] that a linear chain of intersecting spheres has the same depolarization coefficients as an infinite cylinder (within the dipole approximation) [36] for $\xi = [4\sum_{k=1}^{\infty}k^{-3}]^{1/3} \approx 1.688$. This value is close to the one obtained above. It is important to note that two independent depolarization coefficients can simultaneously be "tuned" to correct values by adjusting only one free parameter ξ. As well known, the depolarization coefficients in ellipsoids (an infinite cylinder being a particular case) determine the spectral positions of the resonances. Thus, the renormalization procedure gives the correct spectral locations of the optical resonances for a one-dimensional chain. The lineshape of each resonance can be still described incorrectly. However, in the situation of a large fractal cluster, typical absorption and extinction spectra are superpositions of many collective resonances, and the lineshapes of individual resonance are of little importance.

C. The quasistatic limit

The quasistatic limit plays an important role for the long-wavelength electromagnetic properties of soot. This approximation is highly accurate in the spectral range under consideration ($0.6\mu\text{m} < \lambda < 1\text{cm}$) and provides valuable mathematical simplifications.

When the wavelength is much larger than all characteristic sizes of the system, the terms proportional to x^{-1}, x^{-2} in (6), (7) can be omitted, $\exp(ix)$ set to unity and the incident wave in the right-hand side of (4) replaced by a constant field $\mathbf{E}_0$. The resulting equation can be written in the operator form as

$$|d\rangle = \alpha\left(|E_{\text{inc}}\rangle + W|d\rangle\right) . \tag{17}$$

where $|d\rangle$ is the $3N$-dimensional vector of dipole moments with components $\langle i\alpha|d\rangle = d_{i\alpha}$, and, analogously, $|E_{\text{inc}}\rangle$ is the vector of the incident fields with $\langle i\alpha|E_{\text{inc}}\rangle = E_{0\alpha}$. The $3N \times 3N$-dimensional operator W is real and symmetric in the quasistatic limit, and therefore Hermitian. Its matrix elements are given by

$$\langle i\alpha|W|i\beta\rangle = -\frac{\delta_{\alpha\beta}}{|\mathbf{r}_i - \mathbf{r}_j|^3} + \frac{3(\mathbf{r}_i - \mathbf{r}_j)_\alpha (\mathbf{r}_i - \mathbf{r}_j)_\beta}{|\mathbf{r}_i - \mathbf{r}_j|^5} . \tag{18}$$

Equation (17) can be formally solved using the spectral theorem as [10, 11]

$$|d\rangle = \sum_n \frac{|n\rangle\langle n|E_{\text{inc}}\rangle}{1/\alpha - w_n} , \tag{19}$$

where $|n\rangle$ are the eigenvectors of W with corresponding eigenvalues w_n. The expression for the extinction cross section (8) takes the form

$$\sigma_e = \frac{4\pi k}{|\mathbf{E}_0|^2}\text{Im}\langle E_{\text{inc}}|d\rangle = \frac{4\pi kv}{|\mathbf{E}_0|^2}\text{Im}\sum_n \frac{\langle E_{\text{inc}}|n\rangle\langle n|E_{\text{inc}}\rangle}{1/\chi - vw_n} , \tag{20}$$

where we have used (11) for $1/\alpha$ and neglected, in the quasistatic limit, the term $2k^3/3$.

In the limit $k \to 0$, the expressions (8) and (9) are exactly equal [10, 11]. Therefore, the scattering cross section is zero in this limit. However, σ_s can be calculated in a higher order perturbation expansion where $2k^3/3$ is considered to be a small parameter. If there is no antisymmetrical states in the system [37, 38], or if the absorption parameter $3y_a/2k^3$ is large, the integral scattering cross section is given by

$$\sigma_s = \frac{8\pi k^4}{3|\mathbf{E}_0|^2}|\mathbf{D}|^2 , \tag{21}$$

where $\mathbf{D} = \sum_i \mathbf{d}_i$ is the total dipole moment of a cluster. The above conditions typically hold for carbon soot clusters. For example, for $\lambda = 1\text{cm}$ and $R_m = 50\text{nm}$ we have $3y_a/2k^3 \approx 10^{10}$. This allows us to use expression (21) which implies that the whole cluster radiates as a single dipole.

The expression for $|\mathbf{D}|^2$ can be obtained by using the "homogeneous" vectors $|O_\alpha\rangle$ with components $\langle i\beta|O_\alpha\rangle = \delta_{\alpha\beta}$ by observing that $D_\alpha = \langle O_\alpha|d\rangle$. This leads to

$$\sigma_s = \frac{8\pi k^4 v^2}{3|\mathbf{E}_0|^2}\sum_{\alpha,m,n}\frac{\langle E_{\text{inc}}|m\rangle\langle m|O_\alpha\rangle\langle O_\alpha|n\rangle\langle n|E_{\text{inc}}\rangle}{(1/\chi^* - vw_m)(1/\chi - vw_n)} . \tag{22}$$

D. Weighted density of states and the step-function approximation

In the quasistatic limit, the extinction cross section can be averaged over spatial rotations of a cluster by taking arithmetic average of the corresponding expressions for three orthogonal polarizations of the incident field [10, 11]. Mathematically, this can be expressed as

$$\bar{\sigma}_e = \frac{4\pi kv}{3}\text{Im}\sum_{n,\alpha}\frac{\langle O_\alpha|n\rangle\langle n|O_\alpha\rangle}{1/\chi - vw_n} , \tag{23}$$

where the bar denotes the rotational averaging. Now we introduce the weighted densities of states (WDS) $\Gamma_{\alpha\beta}(w)$ and $\Gamma(w)$ according to

$$\Gamma_{\alpha\beta}(w) = \frac{1}{N}\sum_n \langle O_\alpha|n\rangle\langle n|O_\beta\rangle\delta(w - w_n) , \tag{24}$$

$$\Gamma(w) = \frac{1}{3}\sum_\alpha \Gamma_{\alpha\alpha}(w) . \tag{25}$$

Then (23) can be written as

$$\bar{\sigma}_e = 4\pi kV_{\text{tot}}\text{Im}\int_{-\infty}^{\infty}\frac{\Gamma(w)dw}{1/\chi - vw} . \tag{26}$$

Analogously, the expression for the scattering cross section averaged over rotations can be written in terms of the WDS as

$$\bar{\sigma}_s = \frac{8\pi k^4 V_{\text{tot}}^2}{9}\sum_{\alpha\beta}\int_{-\infty}^{\infty}\frac{\Gamma_{\beta\alpha}(w_1)\Gamma_{\alpha\beta}(w_2)dw_1 dw_2}{(1/\chi^* - vw_1)(1/\chi - vw_2)} . \tag{27}$$

The normalization rules for the WDS are

$$\int_{-\infty}^{\infty}\Gamma_{\alpha\beta}(w)dw = \delta_{\alpha\beta} . \tag{28}$$

For spherically symmetrical, on average, clusters, we can assume that, in the first approximation, $\Gamma_{\alpha\beta}(w) = \delta_{\alpha\beta}\Gamma(w)$. Then (26) turns to

$$\bar{\sigma}_s = \frac{8\pi k^4 V_{\text{tot}}^2}{3}\left|\int_{-\infty}^{\infty}\frac{\Gamma(w)dw}{1/\chi - vw}\right|^2 . \tag{29}$$

The WDS calculated for an ensemble of 10 random cluster-cluster aggregates with $N = 1,000$ particles in each aggregate and fractal dimension $D \approx 1.8$ is shown in Fig. 4 as a function of the dimensionless variable vw. The solid line is obtained by exact diagonalization of W (18) and smoothing $\Gamma(w)$ over small intervals Δw. The dashed line is the step function approximation of the WDS which is discussed in detail below.

By comparing Figs. 4 and 2, we see that the the spectral variable $1/\chi$ does not effectively probe the detailed structure of $\Gamma(w)$ when we tune λ. This indicates that the complicated structure of $\Gamma(w)$ with multiple maxima and minima is of little importance. In the simplest case, one can replace $\Gamma(w)$ by a delta-function, which is equivalent to making the mean-field approximation. However, the mean-filed approximation is inaccurate in the long-wavelength limit because the variable $1/\chi$ approaches the real axis for $\lambda > 10\mu\text{m}$ and the distance $|1/\chi - wv|$ becomes comparable with the effective width of $\Gamma(w)$.

The next level of approximation is to replace $\Gamma(w)$ by a step function. Such approximation is shown in Fig. 4 by the dashed line which preserves the normalization, the first and second moments of the exact WDS. Note also that the third moment of $\Gamma(w)$ was numerically found to be very small, so that the step function shown in Fig. 4 effectively conserves the third moment

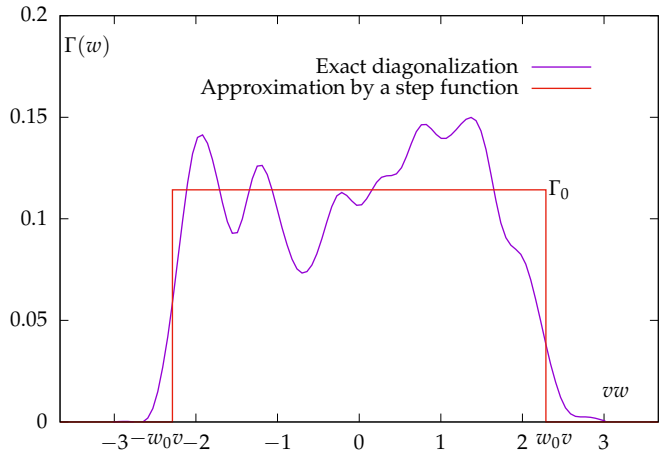

Fig. 4. Weighted density of states $\Gamma(w)$ and its approximation by a step function with the equivalent normalization, first and second moments. The numerical diagonalization is performed for an ensemble of 10 clusters with $N = 1,000$. The values of the constants are $vw_0 = 2.29$ and $\Gamma_0 = 1/2w_0$.

too. Here the constant vw_0 was numerically estimated to be $vw_0 \approx 2.29$, and $\Gamma_0 = 1/2w_0$. The quantity vw_0 is independent of the system dimensions (such as R_m or l), as one could expect in the quasistatic limit.

Given the step function approximation for the WDS, it is easy to obtain analytical expressions for the optical cross sections. A direct integration according to (26),(29) yields for the extinction and scattering cross sections:

$$\bar{\sigma}_e = \frac{2\pi k V_{\text{tot}}}{vw_0}\left(\arctan\frac{X+vw_0}{\delta} - \arctan\frac{X-vw_0}{\delta}\right), \quad \textbf{(30)}$$

$$\bar{\sigma}_s = \frac{2\pi k^4 V_{\text{tot}}^2}{3(vw_0)^2}\left[\frac{1}{4}\ln^2\frac{(X+vw_0)^2+\delta^2}{(X-vw_0)^2+\delta^2} + \left(\arctan\frac{X+vw_0}{\delta} - \arctan\frac{X-vw_0}{\delta}\right)^2\right]. \quad \textbf{(31)}$$

Now we discuss renormalization of the parameters v and w_0 under the set of transformations defined by (12-14). It is easy to see that the renormalized volume is $v' = v(\xi/2)^{3D/(3-D)}$. In general, the eigenvalues of the interaction operator W do not scale with the parameter l, and it is impossible to write a similar relation between w_n and w'_n. However, this becomes possible in the quasistatic limit. Then, from the quasistatic expression (18), it follows that $w'_n = w_n(l/l')^3 = w_n(2/\xi)^{9/(3-D)}$. Combining these two expressions, we obtain $v'w'_n = vw_n(2/\xi)^3$. Therefore, the same transformation applies to vw_0: $v'w'_0 = vw_0(2/\xi)^3$. As could be expected, this transformation does not depend on the fractal dimension D. However, the dependence on D and other geometrical characteristics of a cluster is retained in the eigenvalues calculated *before* the renormalization, i.e., in the constant vw_0. Thus, the intersection procedure effectively increases the normalized eigenvalues and, consequently, the interaction strength. The same tendency holds beyond the quasistatic limit, although the ratio $v'w'_n/vw_n$ becomes different for different n in this case.

In summary, to use the GCRM we simply have to replace the constant vw_0 in (30) and (31) by $vw_0(2/\xi)^3$, where vw_0 must be calculated numerically *before* the renormalization in an ensemble of clusters of touching spheres (i.e., with $l = 2R_m$). The constant vw_0 carries essential information about the cluster geometry. For the cluster-cluster aggregates generated in the Meakin model [30, 31] with mass-independent sub-cluster mobility we estimated $D \approx 1.8$ and $vw_0 \approx 2.29$. It is well known that the fractal dimension can depend on the details of the aggregation process. In particular, the dependence of mobility of sub-clusters on their mass can influence D. In the limiting case when only sub-clusters built of just one monomer can move (the Witten-Sander model [39]), a fixed center of aggregation is formed and the fractal dimension is $D \approx 2.5$ (for clusters embedded in 3D space). We expect that the constant vw_0 will also depend on the details of aggregation. Further investigation is required to establish the dependence of vw_0 on the aggregation model and wether there is a one-to-one correspondence between vw_0 and D.

3. RESULTS

A. Numerical calculations and comparison to experiment

To verify the validity of analytical formulas (30) and (31) we have generated on a computer an ensemble of 10 cluster-cluster aggregates with $N = 1,000$ in each on a simple cubic lattice. We have diagonalized the quasistatic interaction matrix W (18) and calculated the extinction and scattering cross sections according to (20) and (22). The results were averaged over cluster orientations as described in section 2D. We have used the GCRM with $\xi = (4\pi/3)^{1/3} \approx 1.612$. The constants R_m and l were renormalized according to (12),(14). Note that the specific extinction ε_e does not depend in the quasistatic limit on the absolute values of R_m and l but only on their ratio; the same is true for the specific scattering ε_s normalized by k^3V_{tot}. It has been also verified [23] that ε_e only very weakly depends on N and, therefore, on V_{tot} in the quasistatic limit, as long as N is large enough for the fractal geometry to be manifested. Since it is the case for $N = 1,000$, there was no need to renormalize the constant N according to (13). (We emphasize that this is valid only in the quasistatic limit. The GCRM is more general and can be used beyond the quasistatics in which case the dependence on N can be non-trivial and all three renormalization formulas (12-14) must be used simultaneously.)

The results for the specific extinction ε_e and normalized specific scattering $\varepsilon_s/k^3V_{\text{tot}}$ are shown in Figs. 5 and 6. For comparison, we also plot in this figures the corresponding values for unaggregated particles (or in the "noninteracting" limit): $\varepsilon_e^{(\text{nonint})} = 4\pi k\text{Im}\chi$ and $\varepsilon_s^{(\text{nonint})}/k^3V_{\text{tot}} = (8\pi/3)k|\chi|^2$. Note that the same "noninteracting" expressions can be obtained in the Rayleigh-Gans (or, equivalently, first Born) approximation. An excellent agreement between numerical and analytical results (with the interactions included) is apparent. At the same time, the "noninteracting" approximation is seen to become increasingly inaccurate when we move from the near to far IR. A slightly less accurate fit is obtained for the specific scattering. This is explained by the fact that in the derivation of (31) we assumed that the clusters are spherically symmetrical. This is true only on average, while each individual cluster can deviate from the spherical symmetry. As a result, the off-diagonal terms in (27), which are neglected in the further derivations, are not exactly zero.

In Fig. 7 we compare the analytical formula (30) with the experimental measurements of the specific extinction by Bruce *et al.* [9]. Again, the curve illustrating the "noninteracting" limit is also shown for comparison. The experimental data in Ref. [9] are per unit of mass rather than volume. We treated the

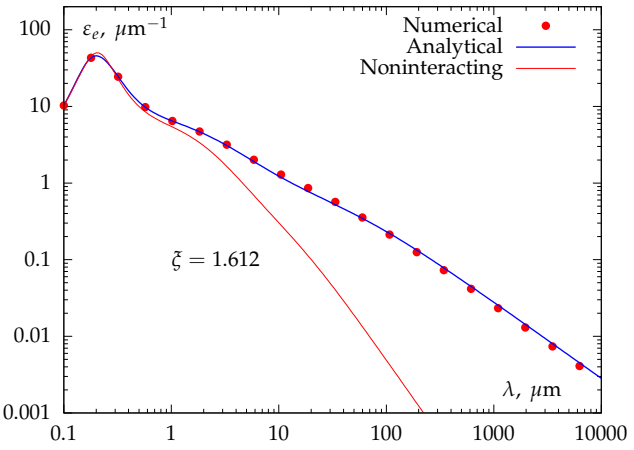

Fig. 5. Specific extinction ε_e calculated numerically (solid line) and according to the analytical approximation (30) (circles). The "noninteracting" limit $\varepsilon_e^{(\mathrm{nonint})} = 4\pi k \mathrm{Im}\chi$ is shown by the thin red line.

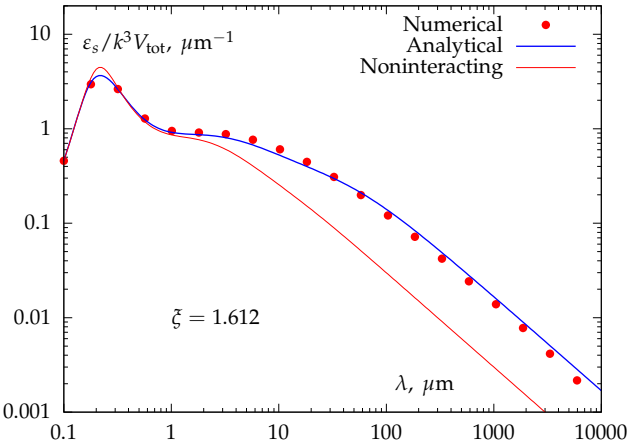

Fig. 6. Specific scattering ε_s normalized by k^3V_{tot} calculated numerically (solid line) and according to the analytical approximation (31) (circles). The "noninteracting" limit $\varepsilon_s^{(\mathrm{nonint})}/k^3V_{\mathrm{tot}} = (8\pi/3)k\,|\chi|^2$ is shown by the thin red line.

mass density of black carbon ρ as an adjustable parameter and found that the best fit (excluding the last experimental point at $\lambda = 8750\mu$m) is achieved for $\rho \approx 1.9\mathrm{g/cm}^3$. This is a reasonable estimate, although the experimental value of ρ in Ref. [9] is not known. (Compare to the following values: graphite - 2.26g/cm^3, buckminster fullerine - 1.69g/cm^3, glassy carbon - from 1.42g/cm^3 to 1.54g/cm^3.) Note that ρ enters all expressions as a constant factor and does not influence the form of the wavelength dependence of ε_e.

The surprisingly good agreement of experimental measurements with the analytical formula, and the reasonable value of ρ obtained suggest that the GCRM gives accurate results for carbonaceous soot. We believe that the small deviations seen in Fig. 7 are due to the insufficient accuracy of the dispersion formula (1) that was used in all calculations. In particular, the apparently unmonotoneous behavior near $\lambda = 500\mu$m can be explained by the presence of an optical resonance at that wavelength; however, (1) does not contain the corresponding term. The same can be true at $\lambda \approx 1$cm where the monotoneous behavior of ε_e is again interrupted. The optical resonance at this wavelength can occur, for example, due to interaction with low-frequency acoustical phonons.

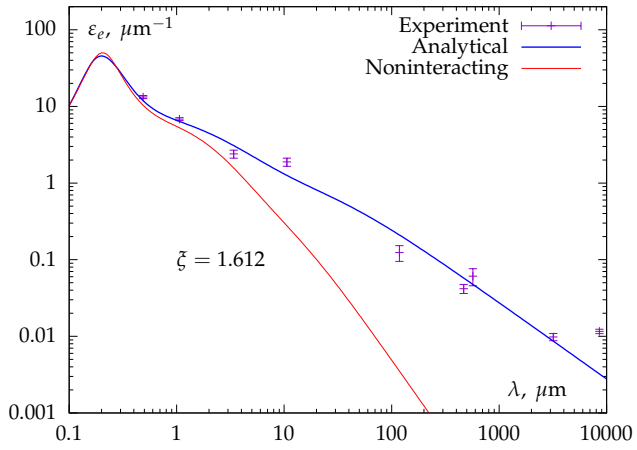

Fig. 7. Specific extinction ε_e calculated according to the analytical approximation (30) compared to experimental values adapted from Bruce *et al.* [9]. The mass density of black carbon of $\rho = 1.9\mathrm{g/cm}^3$ was used to convert the experimental data of Ref. 9 to the units shown in the figure. The "noninteracting" limit $\varepsilon_e^{(\mathrm{nonint})} = 4\pi k \mathrm{Im}\chi$ is shown by the thin red line.

To conclude this section, we note that the computer-generated samples used for numerical calculation of the WDS were built on a cubic lattice. However, in real aggregates, monomers do not occupy lattice sites. The effect of using off-latice aggregates in the computer simulations is not expected to be large and will be addressed by us in the future.

B. Long-wavelength optical properties of soots built from Drudean materials

In this subsection we consider fractal clusters built of a general class of materials who's optical properties are dominated by free electrons. We already saw that this is the case in black carbon for $\lambda > 100\mu$m. We will assume the idealized Drudean form of the dielectric function

$$\epsilon = 1 - \frac{\omega_p^2}{\omega(\omega + i\gamma)} \tag{32}$$

and study the asymptotic behavior of the specific extinction and scattering using the analytical expressions (30) and (31) together with the GCRM. As was discussed in section 2D, application of the GCRM results in the transformation $vw_0 \to vw_0(2/\xi)^3$ in the right-hand side of (30) and (31). We will use the notation $C = vw_0(2/\xi)^3$.

We start with the specific extinction $\varepsilon_e = \bar{\sigma}_e/V_{\mathrm{tot}}$. In the limit $\omega \to 0$, the asymptotic values of X and δ are

$$X = -X_\infty = -4\pi/3\,, \tag{33}$$

$$\delta = 4\pi\gamma\omega/\omega_p^2\,. \tag{34}$$

Then it follows from (30) that

$$\varepsilon_e = \frac{2\pi k}{C}\left(\arctan\frac{C + X_\infty}{\delta} + \mathrm{sgn}(C - X_\infty)\arctan\frac{|C - X_\infty|}{\delta}\right). \tag{35}$$

In the limit $\delta \ll |C - X_\infty|$ this turns to

$$\varepsilon_e = \frac{2\pi k}{C}\left[\frac{\pi}{2}\left(1+\mathrm{sgn}(C-X_\infty)\right) -\delta\left(\frac{1}{C+X_\infty}+\frac{\mathrm{sgn}(C-X_\infty)}{|C-X_\infty|}\right)\right]. \quad (36)$$

We can identify two separate cases. If $C > X_\infty$, the asymptotic form of ε_e is

$$\varepsilon_e = \frac{2\pi^2 k}{C} \propto \frac{1}{\lambda}, \quad \text{if } C > X_\infty . \quad (37)$$

In the opposite case we have

$$\varepsilon_e = \frac{(4\pi)^2 \gamma k \omega}{\omega_p^2 (X_\infty^2 - C^2)} \propto \frac{1}{\lambda^2}, \quad \text{if } C < X_\infty , \quad (38)$$

where we have used expression (34) for δ.

We can define the *critical value* of the parameter vw_0 determined by the condition $C = X_\infty$, or

$$(vw_0)_c = \frac{4\pi}{3}\left(\frac{\xi}{2}\right)^3 . \quad (39)$$

If the geometry of clusters is such that $vw_0 < (vw_0)_c$, the asymptote (38) is valid. The $1/\lambda^2$ behavior is characteristic to noninteracting monomers (e.g., in disaggregated samples). Therefore, we conclude that in the case $vw_0 < (vw_0)_c$ the EM interaction is not important in the long-wavelength regime. In the opposite case the asymptote (37) is valid, and the EM interaction stays important up to the electrostatic limit $\omega = 0$ which is manifested in the $1/\lambda$ dependence.

The asymptotes (37) and (38) are valid only when $\delta \ll |C - X_\infty|$. If the quantity $|C - X_\infty|$ is itself small, the asymptotic behavior of ε_e is manifested only for λ's sufficiently large for the above inequality to be true. In the case $C = X_\infty$, the spectral behavior of ε_e is more complicated. In particular, higher order terms must be retained in the expression (33) for X.

In our calculations illustrated in the previous subsection, the numerically estimated value $vw_0 \approx 2.29$ was larger than the critical value $(vw_0)_c \approx 2.19$ (assuming $\xi = 1.612$). Indeed, the onset of the $1/\lambda$ asymptote can be seen in Figs. 5-7 for $\lambda > 100\mu$m. This means that in the carbon smoke with the geometry of cluster-cluster aggregates ($D \approx 1.8$) and optical constants specified in section 1B, the EM interaction is always important in the long-wavelength limit. We believe that the value of ξ, and, consequently, of the critical constant $(vw_0)_c$, are universal for a broad class of soots. However, the quantity vw_0 can strongly depend on the sample geometry. Further investigation is required to establish the numerical value of $(vw_0)_c$ with a higher accuracy and to verify the analytical results for materials with different parameters vw_0, γ and ω_p.

The mean-field approximation can be obtained from (30) by either considering the limit of infinitely narrow WDS ($w_0 \to 0$) or large absorption ($\gamma \to \infty$). In the first case we obtain $\varepsilon_e = 4\pi k \mathrm{Im}\chi$ and in the second case $\varepsilon_e = 4\pi k/\delta$. Obviously, the latter formula can be obtained from the former by taking the limit $\delta \gg |X|$. Note that in the quasistatic limit the mean-field and the first Born approximations are equivalent due to the symmetry of the dipole interaction in the near zone.

Now we turn our attention to the specific scattering, ε_s. Applying similar analysis to Eq. (30) and assuming that $\delta \ll |C - X_\infty|$, we obtain

$$\frac{\varepsilon_s}{k^3 V_{\mathrm{tot}}} = \frac{2\pi k}{3C^2}\left[\ln^2\frac{C-X_\infty}{C+X_\infty} + \left(\frac{\pi}{2}\right)^2\right], \quad \text{if } C > X_\infty ; \quad (40)$$

$$\frac{\varepsilon_s}{k^3 V_{\mathrm{tot}}} = \frac{2\pi k}{3C^2}\left[\ln^2\frac{X_\infty - C}{X_\infty + C} + \frac{(2C\delta)^2}{(X_\infty^2 - C^2)^2}\right], \quad \text{if } C < X_\infty . \quad (41)$$

Note that ε_e is proportional to V_{tot}. Therefore, the total power of scattered light depends on how the soot material is divided between individual clusters, assuming that the total concentration of the soot material in the scattering volume is fixed. In the case $C > X_\infty$ the long-wavelength asymptote for the specific scattering is $\varepsilon(\lambda) \propto 1/\lambda^4$. In the opposite case ($C < X_\infty$), the asymptote is more complicated and includes two competing terms $\propto 1/\lambda^4$ and $\propto 1/\lambda^6$. The last term is characteristic to noninteracting monomers and is dominating in the limit $C \to 0$ or $\gamma \to \infty$, when the mean-field approximation becomes accurate.

4. SUMMARY AND DISCUSSION

We have built a theory of long-wavelength optical properties of fractal clusters with optical constants that are dominated by the input of free electrons in the $\lambda \to \infty$ limit. Analytical expressions were derived for the extinction and scattering cross sections. The theory was applied to fractal carbonaceous soot, and the results verified by comparison with experimental measurements in a wide spectral range.

Although the carbonaceous soot was the main focus of this paper, our approach is of a more general applicability. We have made three main approximations, all of which proved to be very accurate for the object under investigation, but are essentially independent of each other. These approximations are (i) the geometrical renormalization of clusters, (ii) the quasistatic approximation, and (iii) replacing the weighted density of states by a step function.

The geometrical cluster renormalization method (GCRM) is applicable beyond the quasistatics, when the retardation effects are fully included in the consideration. It also does not put any explicit restrictions on the geometry of samples (as long as they are fractal with $D < 3$) or the refractive index of the material, although this topic is insufficiently investigated at the present time. The quasistatic approximation is, clearly, applicable when the clusters are small compared to the wavelength, but can be also very accurate in large clusters with low fractal dimensions [12] because the near-zone EM interaction is fast decaying as $1/r^3$. Finally, the step-function approximation is applicable only when certain mathematical relations between the WDS and the complex spectral variable $1/\chi$ hold. Thus, it puts restrictions on the refractive index and/or geometry. However, it can be applied beyond the quasistatic limit, although the analytical expressions in this case become more cumbersome.

We showed that the asymptotic form of the specific extinction $\varepsilon_e(\lambda)$ in the limit $\lambda \to \infty$ can be either $1/\lambda$ or $1/\lambda^2$. The cross-over between these two regimes has the nature of a critical phenomenon and is governed by the parameter vw_0 that characterizes the effective width of the WDS. We have identified the critical value of this parameter, $(vw_0)_c$.

This research was supported by Battelle under Contract DAAH04-96-C-0086. It was also partially supported by National Computational Science Alliance under Grant PHY980006N and utilized the NCSA HP/Convex Exemplar SPP-2000, by the NSF under grant DMR-9810183 and by the ARO under grant DAAG55-98-1-0425). The authors are grateful to C. Bruce for very useful discussions and to D. Mackowski for making available his Fortran codes.

REFERENCES

1. S. R. Forrest and T. A. Witten, "Long-range correlations in smoke-particle aggregates," J. Phys. A **12**, L109–L117 (1979).
2. H. X. Zhang, C. M. Sorensen, E. R. Ramer, B. J. Olivier, and J. F. Merklin, "In sutu optical structure factor measurements of an aggregating soot aerosol," Langmuir **4**, 867–871 (1988).
3. U. O. Koylu and G. M. Faeth, "Structure of overfire soot in buoyant turbulent diffusion flames at long residence times," Combust. Flame **89**, 140–156 (1992).
4. J. Cai, N. Lu, and C. M. Sorensen, "Comparison of size and morphology of soot aggregates as determined by light scattering and electron microscope analysis," Langmuir **9**, 2861–2867 (1993).
5. M. V. Berry and I. C. Percival, "Optics of fractal clusters such as smoke," Opt. Acta **33**, 577–591 (1986).
6. W. H. Dalzell and A. F. Sarofim, "Optical constants of soot and their application to heat-flux calculations," J. Heat Transf. **91**, 100–104 (1969).
7. G. W. Mulholland, C. F. Bohren, and K. A. Fuller, "Light scattering by agglomerates: Coulped electric and magnetic dipole method," Langmuir **10**, 2533–2546 (1994).
8. D. W. Mackowski, "Electrostatics analysis of radiative absorption by sphere clusters in the rayleigh limit: Application to soot particles," Appl. Opt. **34**, 3535–3545 (1995).
9. C. W. Bruce, T. F. Stromberg, K. P. Gurton, and J. B. Mozer, "Transspectral absorption and scattering of electromagnetic radiation by disel soot," Appl. Opt. **30**, 1537–1546 (1991).
10. V. A. Markel, L. S. Muratov, and M. I. Stockman, "Optical properties of fractals: Theory and numerical simulation," J. Exp. Theor. Phys. **71**, 455–464 (1990).
11. V. A. Markel, L. S. Muratov, M. I. Stockman, and T. F. George, "Theory and numerical simulation of optical properties of fractal clusters," Phys. Rev. B **43**, 8183–8195 (1991).
12. V. M. Shalaev, R. Botet, and R. Jullien, "Resonant light scattering by fractal clusters," Phys. Rev. B **44**, 12216–12225 (1991).
13. V. M. Shalaev, *Nonlinear Optics of Random Media: Fractal Composites and Metal Dielectric Films* (Springer Verlag, Berlin, 2000).
14. J. M. Gerardy and M. Ausloos, "Absorption spectrum of clusters of spheres from the general solution of Maxwell's equations. The long-wave limit," Phys. Rev. B **22**, 4950–4959 (1980).
15. F. Claro, "Absorption spectrum of neighboring dielectric grains," Phys. Rev. B **25**, R7875–R7876 (1982).
16. R. Rojas and F. Claro, "Electromagnetic response of an array of particles: Normal-mode theory," Phys. Rev. B **34**, 3730–3736 (1986).
17. K. A. Fuller, "Scattering and absorption cross sections of compounded spheres. I. Theory for external aggregation," J. Opt. Soc. Am. A **11**, 3251–3260 (1994).
18. F. J. G. de Abajo, "Interaction of radiation and fast electrons with clusters and dielectrics: A multiple scattering approach," Phys. Rev. Lett. **82**, 2776–2779 (1999).
19. F. J. G. de Abajo, "Multiple scattering of radiation in clusters of dielectrics," Phys. Rev. B **60**, 6086–6102 (1999).
20. J. E. Sansonetti and J. K. Furdyna, "Depolarization effects in arrays of spheres," Phys. Rev. B **22**, 2866–2874 (1980).
21. F. Claro, "Theory of resonant modes in particulate matter," Phys. Rev. B **30**, 4989–4999 (1984).
22. F. Claro, "Multipolar effects in particulate matter," Solid State Comm. **49**, 229–232 (1984).
23. V. A. Markel, V. M. Shalaev, E. B. Stechel, W. Kim, and R. L. Armstrong, "Small-particle composites. I. Linear optical properties," Phys. Rev. B **53**, 2425–2436 (1996).
24. V. A. Markel and V. M. Shalaev, Computational approaches in optics of fractal clusters, in *Computational Studies of New Materials* pp. 210–243 (World Scientific, Singapore, 1999).
25. E. A. Taft and E. A. Philipp, "Optical properties of graphite," Phys. Rev. **138**, A197–A202 (1965).
26. Z. G. Habib and P. Vervisch, "On the refractive index of soot at flame temperatures," Combust. Sci. Tech. **59**, 261–274 (1988).
27. S. C. Lee and C. L. Tien, "Optical constants of soot in hydrocarbon flames," in *Eighteenth Symposium (International) on Combustion*, pp. 1159–1166 (The Combustion Institute, 1981).
28. X and δ used in Refs. [10, 11] differ from the dimensionless parameters defined below by a multiplicative factor with dimensionality of length cubed.
29. D. W. Mackowski, "Calculation of total cross sections of multiple-sphere clusters," J. Opt. Soc. Am. A **11**, 2851–2861 (1994).
30. P. Meakin, "Formation of fractal clusters and networks by irreversible diffusion-limited aggregation," Phys. Rev. Lett. **51**, 1119–1122 (1983).
31. R. Jullien, M. Kolb, and R. Botet, "Aggregation by kinetic clustering of clusters in dimensions $d > 2$," J. Physique Lett. **45**, L211–L216 (1984).
32. B. T. Draine, "The discrete-dipole approximation and its application to interstellar graphite grains," Astrophys. J. **333**, 848–872 (1988).
33. E. M. Purcell and C. R. Pennypacker, "Scattering and absorption of light by nonspherical dielectric grains," Astrophys. J. **186**, 705–714 (1973).
34. B. Draine and P. Flatau, "Discrete-dipole approximation for scattering calculations," J. Opt. Soc. Am. A **11**, 1491–1499 (1994).
35. V. A. Markel, "Coupled-dipole approach to scattering of light from a one-dimensional periodic dipole chain," J. Mod. Opt. **40**, 2281–2291 (1993).
36. A finite linear chain of touching spheres with multipole interaction was considered by Mackowski [8]. It was found numerically that, in general, such chain is not equivalent to a spheroid with the same aspect ratio. The intersection parameter which gives the same depolarization coefficient for an infinite chain of spheres as in an infinite cylinder may be different with the multipole interactions included than in the dipole approximation.
37. V. A. Markel, "Scattering of light from two interacting spherical particles," J. Mod. Opt. **39**, 853–861 (1992).
38. V. A. Markel, "Antisymmetrical optical states," J. Opt. Soc. Am. B **12**, 1783–1791 (1995).
39. T. A. Witten and L. M. Sander, "Diffusion-limited aggregation, a kinetic critical phenomenon," Phys. Rev. Lett. **47**, 1400–1403 (1981).